

Magnetic Field Simulations Using Explicit Time Integration With Higher Order Schemes

Bernhard Kähne*, Markus Clemens* and Sebastian Schöps†

*University of Wuppertal, Chair for Electromagnetic Theory, Rainer-Gruenter-Str. 21, 42119 Wuppertal, Germany

† Graduate School of Computational Engineering, Technical University of Darmstadt, 64293 Darmstadt, Germany

E-mail: kaehne@uni-wuppertal.de

Abstract—A transient magneto-quasistatic vector potential formulation involving nonlinear material is spatially discretized using the finite element method of first and second polynomial order. By applying a generalized Schur complement the resulting system of differential algebraic equations is reformulated into a system of ordinary differential equations (ODE). The ODE system is integrated in time using the explicit Euler scheme, which is conditionally stable by a maximum time step size. To overcome this limit, an explicit multistage Runge-Kutta-Chebyshev time integration method of higher order is employed to enlarge the maximum stable time step size. Both time integration methods are compared regarding the overall computational effort.

Index Terms—Eddy currents, explicit Euler scheme, Runge-Kutta-Chebyshev quadrature, transient magneto-quasistatics

I. INTRODUCTION

The simulation of magneto-quasistatic (MQS) field problems is crucial in the design process of electric machines, transformers and any other devices in the low frequency regime. Usually, these applications have material coefficients, which differ by many magnitudes through the computational domain like e.g. the change of the conductivity through the rotor, air-gap and stator of an electric engine. Furthermore, often some conductive parts of the problem are ferromagnetic with a nonlinear B-H-characteristic.

Spatial discretization of MQS field problems based on a magnetic vector potential formulation using the finite element method (FEM) yields nonlinear infinitely stiff differential-algebraic equation (DAE) systems of index 1. This DAE is commonly integrated in time employing implicit integration techniques [1]. A nonlinear system of equations has to be solved by e.g. the Newton-Raphson method, which requires multiple iterations and repeated calculations of the Jacobian matrix in order to carry out one implicit time step. This is computationally expensive, but, due to implicit integration, unconditionally stable with no restriction of the time step size.

In this paper, the DAE system is translated into a system of ordinary differential equations (ODE) using the generalized Schur complement, as was originally presented in [2]. This ODE system is integrated in time by employing the explicit Euler scheme, which is conditionally stable by a maximum time increment according to a Courant-Friedrichs-Levi (CFL) -like criterion. Unlike in the implicit integration scheme, here the use of a linearization scheme is avoided. Hence, one explicit time step is computationally less expensive. Based on previous numerical investigations presented in [3] and [4], this paper presents numerical results for higher order spatial discretizations. Furthermore, a explicit multistage Runge-Kutta-Chebyshev (RKC) method of higher order is employed in order to increase the maximum stable time

step size as presented in [1] and [5]. The RKC method provides to control the maximum stable time step size which is quadratic in the number of stages.

II. MATHEMATICAL FORMULATION

The magnetic flux density \vec{B} is described by the magnetic vector potential \vec{A} such that

$$\vec{B} = \nabla \times \vec{A}. \quad (1)$$

Using the non-gauged magnetic vector potential in \vec{A}^* -formulation, the governing MQS boundary value problem for the computational domain Ω , see Fig. 1, reads

$$\begin{aligned} \nabla \times (\nu \nabla \times \vec{A}(\vec{r}, t)) + \kappa \frac{\partial \vec{A}(\vec{r}, t)}{\partial t} &= \vec{J}(\vec{r}, t) \quad \forall \vec{r} \in \Omega, \\ \vec{n} \times \vec{A}(\vec{r}, t) &= 0 \quad \forall \vec{r} \in \partial\Omega \end{aligned} \quad (2)$$

where ν is the nonlinear reluctivity, typically dependent on \vec{B} , κ is the electrical conductivity and \vec{J} is current density. The corresponding variational formulation of (2) reads: find $\vec{A} \in \mathcal{H}_0(\mathbf{curl}, \Omega)$ such that

$$\begin{aligned} \int_{\Omega} \kappa \frac{\partial \vec{A}}{\partial t} \cdot \vec{w} \, d\Omega + \int_{\Omega} \nu (\nabla \times \vec{A}) \cdot (\nabla \times \vec{w}) \, d\Omega \\ = \int_{\Omega} \vec{J} \cdot \vec{w} \, d\Omega \end{aligned} \quad (3)$$

holds true for all curl-conforming edge element test functions $\vec{w} \in \mathcal{H}(\mathbf{curl}, \Omega)$.

A. Spatial discretization

The vector potential \vec{A} is approximated by a finite set of edge elements:

$$\vec{A} \approx \vec{A}_h = \sum_{i=1}^N a_i \vec{w}_i, \quad (4)$$

where $\vec{w}_i \in \mathcal{H}_0(\mathbf{curl}, \Omega)$ and N denotes the number degrees of freedom (DOF). According to the Galerkin

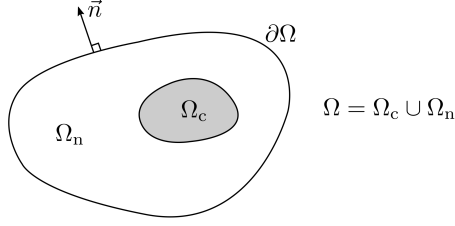


Fig. 1. Computational domain Ω splitted into a conductive Ω_c and a non-conductive Ω_n subdomain with boundary $\partial\Omega$ and outer normal vector \vec{n} .

scheme the test functions are taken from the same basis as \vec{A}_h . Coefficients a_i assigned to the conductive area Ω_c are stored in vector \mathbf{a}_c , likewise vector \mathbf{a}_n holds the coefficients in the nonconducting area Ω_n , see Fig. 1. It follows the DAE system

$$\begin{bmatrix} \mathbf{M}_c & 0 \\ 0 & 0 \end{bmatrix} \frac{d}{dt} \begin{bmatrix} \mathbf{a}_c \\ \mathbf{a}_n \end{bmatrix} + \begin{bmatrix} \mathbf{K}_c(\mathbf{a}_c) & \mathbf{K}_{cn} \\ \mathbf{K}_{cn}^T & \mathbf{K}_n \end{bmatrix} \begin{bmatrix} \mathbf{a}_c \\ \mathbf{a}_n \end{bmatrix} = \begin{bmatrix} 0 \\ \mathbf{j} \end{bmatrix} \quad (5)$$

where \mathbf{M}_c is the positive-definite and symmetric conductivity matrix, \mathbf{K}_c is the time dependent curl-curl matrix in the conductive region and \mathbf{K}_n is the constant curl-curl matrix in the non-conductive area. \mathbf{K}_{cn} is the coupling matrix, which couples the DOF in the conductive area with neighboring DOF in the non-conductive area. The vector \mathbf{j} defined by the right-hand side (RHS) of the variational formulation (3) is only present to the non-conductive region Ω_n . Due to the null-space of the discrete curl-curl operator \mathbf{K}_n , a vanishing weak divergence of \mathbf{j} in Ω_n is crucial for the convergence of iterative solvers having a weak gauging property, e.g. the preconditioned conjugate gradient (PCG) method [6].

Applying the generalized Schur complement

$$\mathbf{K}_S(\mathbf{a}_c) = \mathbf{K}_c(\mathbf{a}_c) - \mathbf{K}_{cn} \mathbf{K}_n^+ \mathbf{K}_{cn}^T \quad (6)$$

where \mathbf{K}_n^+ is the Moore-Penrose pseudo-inverse matrix of the singular curl-curl matrix \mathbf{K}_n , equation (5) decomposes into a finitely stiff ODE system and an algebraic equation given by

$$\mathbf{M}_c \frac{d}{dt} \mathbf{a}_c + \mathbf{K}_S(\mathbf{a}_c) \mathbf{a}_c = -\mathbf{K}_{cn} \mathbf{K}_n^+ \mathbf{j} \quad (7)$$

$$\mathbf{a}_n = \mathbf{K}_n^+ \mathbf{j} - \mathbf{K}_n^+ \mathbf{K}_{cn}^T \mathbf{a}_c. \quad (8)$$

Finally, the system of ODEs (7) has the canonical form

$$\frac{d}{dt} \mathbf{a}_c(t) = \underbrace{-\mathbf{M}_c^{-1} [\mathbf{K}_{cn} \mathbf{K}_n^+ \mathbf{j} + \mathbf{K}_S(\mathbf{a}_c) \mathbf{a}_c]}_{=: \mathbf{f}(t, \mathbf{a}_c(t))}. \quad (9)$$

B. The explicit Euler time integration scheme

Replacing the time derivative in ODE system (9) by the forward discrete difference yields to the explicit Euler scheme. The solution for the $(i+1)$ -th time step reads

$$\mathbf{a}_c^{i+1} = \mathbf{a}_c^i + \tau \mathbf{f}(t^i, \mathbf{a}_c^i), \quad (10)$$

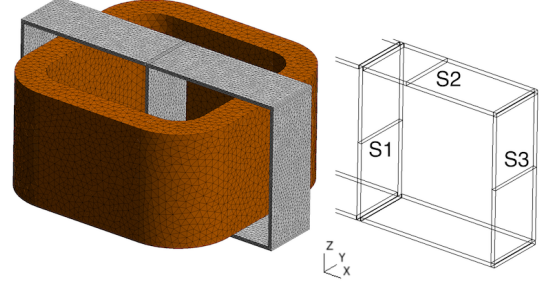


Fig. 2. Left: structure and tetrahedral mesh of the TEAM 10 benchmark problem with about 280 000 elements. Symmetrically placed steel plates (gray) around a coil (brown). Right: cross section S1-S3 of the steel plates with the dimension 3.2 mm \times 50 mm.

where $\tau = t^{i+1} - t^i$ is the time step size. The maximum stable time step size is determined by

$$\tau \leq \frac{2}{\lambda_{\max}(\mathbf{M}_c^{-1} \mathbf{K}_S(\mathbf{a}_c))}, \quad (11)$$

where λ_{\max} is the maximum eigenvalue.

C. The Runge-Kutta-Chebyshev time integration method

Alternatively, the system of ODEs (9) can be integrated explicitly in time by using the RKC method with a number of stages s . In order to compute the $(i+1)$ -th time step the stages have the form

$$\begin{aligned} \mathbf{y}_0 &= \mathbf{a}_c^i \\ \mathbf{y}_1 &= \mathbf{y}_0 + \tilde{\mu}_1 \tau \mathbf{f}_0^i \\ \mathbf{y}_j &= (1 - \mu_j - \nu_j) \mathbf{y}_0 + \mu_j \mathbf{y}_{j-1} + \nu_j \mathbf{y}_{j-2} \\ &\quad + \tilde{\mu}_j \tau \mathbf{f}_{j-1}^i + \tilde{\gamma}_j \tau \mathbf{f}_0^i, \quad j = 2, \dots, s \\ \mathbf{a}_c^{i+1} &= \mathbf{y}_s, \end{aligned} \quad (12)$$

with $\mathbf{f}_j^i = \mathbf{f}(t^i + c_j \tau, \mathbf{y}_j)$. All coefficients appearing in the RKC scheme (12) are given analytically in [5] for an arbitrary number of stages $s \geq 2$. Let T_j be the Chebyshev polynomial of the first kind and degree j . For $2 \leq j \leq s$ the coefficients are

$$\begin{aligned} \tilde{\mu}_1 &= b_1 w_1, \quad \mu_j = \frac{2b_j w_0}{b_{j-1}}, \quad \nu_j = \frac{-b_j}{b_{j-2}}, \\ \tilde{\mu}_j &= \frac{2b_j w_1}{b_{j-1}}, \quad \tilde{\gamma}_j = -(1 - b_{j-1} T_{j-1}(w_0)) \tilde{\mu}_j, \end{aligned} \quad (13)$$

with

$$\begin{aligned} \varepsilon &= \frac{2}{13}, \quad w_0 = 1 + \frac{\varepsilon}{s^2}, \quad w_1 = \frac{T'_s(w_0)}{T''_s(w_0)}, \\ b_j &= \frac{T''_j(w_0)}{(T'_j(w_0))^2}, \quad b_0 = b_2, \quad b_1 = b_2 \end{aligned} \quad (14)$$

and

$$\begin{aligned} c_j &= \frac{T'_s(w_0)}{T''_s(w_0)} \frac{T''_j(w_0)}{T'_j(w_0)} \quad (2 \leq j \leq s-1) \\ c_1 &= \frac{c_2}{T'_2(w_0)}, \quad c_s = 1. \end{aligned} \quad (15)$$

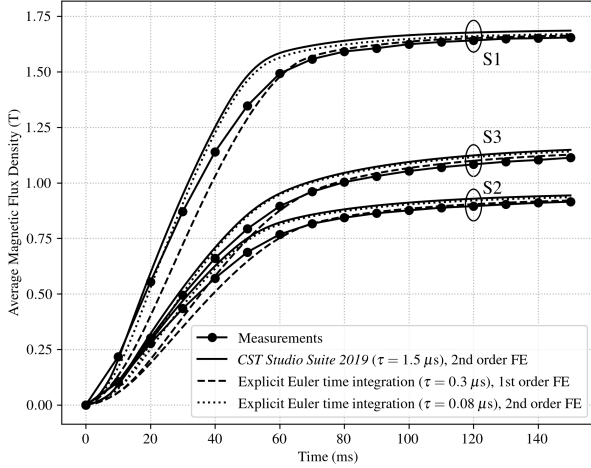


Fig. 3. Results for the average magnetic flux density evaluated at the cross sections S1-S3, see Fig. 2, compared with measurements from [7]. Additional validation with unconditionally stable implicit time integration using *CST Studio Suite 2019* software [9] on a different tetrahedral mesh with about 2 000 000 elements.

The condition for absolute stability is given by

$$\tau \leq 0.653 \cdot \frac{s^2}{\lambda_{\max}(M_c^{-1} K_S(a_c))}. \quad (16)$$

Unlike the stability criterion (11) of the explicit Euler scheme, the maximum stable time increment increases quadratically in the number of stages s .

III. NUMERICAL CASE STUDY

The case study in order to validate the formulations above is the TEAM 10 benchmark problem presented in [7]. It contains symmetrically placed steel plates around a coil, see Fig. 2. At the junction from the center plate to the left and right canal exists air gaps of 0.5 mm. Furthermore, the conductive steel plates have a nonlinear B-H-characteristic. The coil has 162 turns and is excited by a transient current

$$i_S(t) = 5.64 \text{ A} \cdot \left(1 - e^{-\frac{t}{0.5s}}\right). \quad (17)$$

Since the coil is modeled as a stranded conductor, the source current density appearing on the RHS of (2) is described as $\vec{J}(\vec{r}, t) = \vec{X}_S(\vec{r})i_S(t)$, where \vec{X}_S is the spatial current distribution. It is computed using an electric vector potential formulation presented in [8].

In order to evaluate the matrix-vector product with the pseudo-inverse of the matrix K_n in the RHS of ODE (9), a parallel PCG method with Jacobi preconditioner is applied. Since the matrix M_c has full rank, the corresponding system of equations can be solved using a parallel direct solver. The evaluation of the vector potential a_c in the conductive region is independent of the vector potential a_n in the non-conductive region. Thus, the computation of a_n according to equation (8) can be considered as a post-processing step. Furthermore, the matrix vector product $K_n^+ j$ is essentially a linear magneto-static problem in the non-conductive area. Thus,

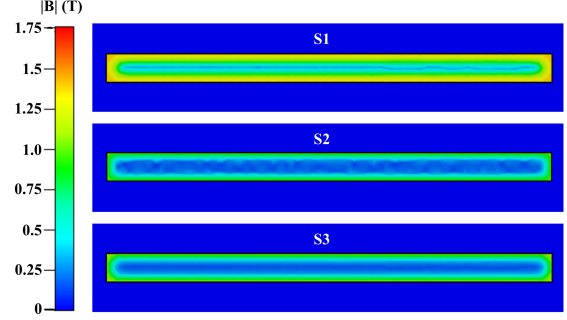


Fig. 4. Illustration of the skin effect inside the conductive parts. The magnetic flux density \vec{B} on cross sections S1-S3, see Fig. 2. Second order FEM solution at time $t = 30$ ms obtained from *CST Studio Suite 2019*.

it is computed only once with $i_S = 1$ A and scaled with $i_S(t)$ by evaluating the canonical RHS f at time t .

Since f is evaluated in each time step at least once, the repetitive evaluation of the pseudo-inverse K_n^+ forms a multiple right-hand side problem, [3]. Therefore, the proper orthogonal decomposition (POD) is used in order to generate improved initial vectors for the PCG method.

A. Update strategy of the time dependent curl-curl matrix

The nonlinear reluctivity $\nu(|\nabla \times \vec{A}|)$ involves an update of the curl-curl matrix $K_c(a_c)$. Due to explicit time integration the curl-curl matrix is evaluated for past instances of the vector potential a_c . Hence, a linearization scheme is avoided. However, the Runge-Kutta stages (12) still require multiple evaluations of K_c per time step which are costly. This approach may therefore become inefficient since the maximal time step size, i.e. (11) and (16), does not reflect the dynamics of the solution. We suggest to bypass evaluations of the nonlinearity material curve.

As proposed in [4] the matrix $K_c(a_c)$ is kept constant for several time steps as long as

$$\frac{\|a_c^* - a_c^i\|}{\|a_c^*\|} \leq tol \quad (18)$$

holds true for a given tolerance tol , where a_c^i is the latest solution and a_c^* denotes the solution at the latest matrix update. In this case study the matrix $K_c(a_c)$ is updated if tol exceeds 0.5%.

B. Numerical results

The FEM simulations according to the formulation above are executed on a tetrahedral mesh with about 280 000 elements. To show convergence for a higher finite element (FE) order, the steel plates of the dimension $3.2 \text{ mm} \times 50 \text{ mm}$, see Fig. 2, are coarsely discretized by an edge length of 3.2 mm, the short side of the steel plates. The first order finite element discretization contains about 300 000 DOF, whereas the second order

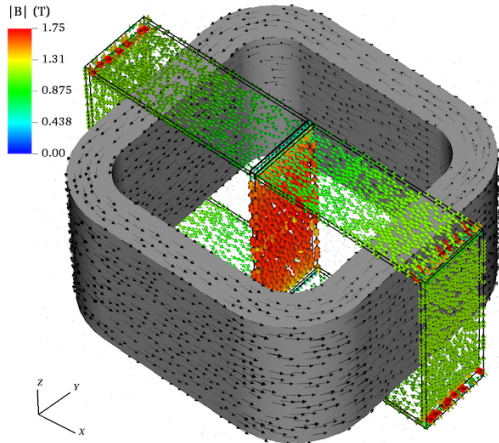


Fig. 5. Vector field plot of the magnetic flux density \vec{B} inside the steel plates (black wire frame) and homogeneous source current density \vec{J} (black arrows) inside the coil (gray solid). Second order FEM solution at time $t = 150$ ms.

discretization results in about 1.8 mio. DOF on the same mesh.

The numerical results using the explicit Euler scheme in comparison to measurements from [7] are depicted in Fig. 3. The quantity under test is the average magnetic flux density evaluated on the cross sections of the steel plates S1-S3, see Fig. 2. Both, for first and second order finite element solutions a good agreement with the measurements is noticeable when the magnetic flux saturates. In the time range $0 \leq t \leq 60$ ms a more significant deviation between the lowest order finite element simulation and the measurements is visible. In order to analyse this behavior a second order FEM simulation using the commercial *CST Studio Suite 2019* software [9] is executed. This involves a different tetrahedral mesh of about 2 000 000 elements where the short side of the steel plates have a finer discretization with four layers of elements. In Fig. 3 the second order finite element solution with the explicit scheme coincides well with the solution obtained from the *CST Studio Suite 2019* software, thus it is taken as reference solution for further investigations.

The deviations of the first order finite element solution to the reference solution is explained by a not sufficient spatial resolution of the skin effect. In this case study the strongest skin effect occurs at time $t = 30$ ms, see Fig. 4. The relative error of the explicit Euler solution using second order finite elements is less than 5%, see TABLE I. Hence, the given mesh resolves the skin effect sufficiently with respect to the error by using second order finite element discretization. However, when the magnetic flux saturates less eddy currents are induced. Hence, the magnetic flux is approximately homogeneous and the coarse spatial discretization by using first order finite elements less affects the numerical error, which is 1.3% at time $t = 150$ ms. Fig. 5 shows the homogenous magnetic flux density in saturation as second order finite

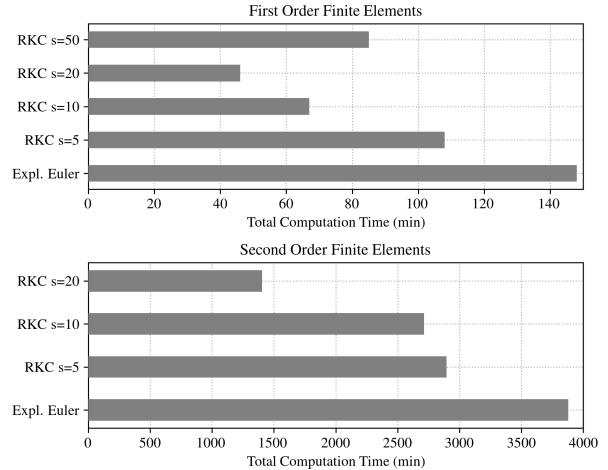


Fig. 6. Total computation time of the explicit Euler scheme and the RKC method with different numbers of stages s for first (top) and second (bottom) finite element order.

element solution, where the relative error is less than 1%.

C. Performance study of the Runge-Kutta-Chebyshev method versus the explicit Euler scheme

A sufficient spatial discretization is crucial to resolve effects caused by induction as are the eddy currents and the skin effect. Due to the stability criterion (11) of the explicit Euler scheme, the time step size decreases quadratically by refining the spatial discretization. The RKC method provides a possibility to compensate the decrease of the maximum stable time increment by choosing a corresponding number of stages s , see equation (16).

Within the Runge-Kutta stages (12), where the canonical RHS \mathbf{f} is evaluated at different time points $t^i + c_j \tau$, $2 \leq j \leq s$ and $c_s = 1$, the time dependent curl-curl matrix $\mathbf{K}_c(\mathbf{a}_c)$ is kept constant without regarding the update strategy described in section III-A. The criterion (18) is only evaluated after a full time step.

Fig. 6 shows the total computation time of the RKC method in comparison with the explicit Euler scheme for first and second order finite elements. As expected, in both cases the explicit Euler scheme features the longest computation times. Employing the RKC method, the total simulation time consumption is diminished significantly for a higher number of stages s . However, s has to be chosen with care as larger time step sizes can trigger the update criterion (18) after each time step, which compromises the overall performance. For this reason, the RKC method with $s = 50$ requires longer computation times than the RKC method with $s = 10$ in the first order finite element setting.

The error of all explicit methods with respect to the reference solution is approximately the same and is mainly given by the error in space. The deviation in the magnetic flux density is about 13% and 4% for first and second order finite elements, respectively, see TABLE I.

TABLE I
RELATIVE ERROR OF EXPLICIT EULER AND RKC SIMULATIONS TO
THE IMPLICIT REFERENCE SOLUTION

Time Integration Scheme	$err = \frac{\ B_{ref} - B\ _{\infty}}{\ B_{ref}\ _{\infty}}$	
	First Order FE	Second Order FE
Expl. Euler	0.13352	0.04168
RKC $s = 5$	0.13347	0.04169
RKC $s = 10$	0.13349	0.04170
RKC $s = 20$	0.13354	0.04172

All computations are executed with 20 parallel MPI processes on a workstation with an *Intel Xeon E5* processor. The C++ library *MFEM* [10] is involved for obtaining the finite element operators, the library *PETSc* [11] provides the parallel PCG solver and the POD method as well as parallel direct solver.

IV. CONCLUSION

For transient nonlinear magneto-quasistatic field simulations, in this paper a magnetic vector potential formulation was discretized using the finite element method of first and second polynomial order and the resulting system of DAEs was transformed into an ODE system employing a generalized Schur complement. This system of ODEs was integrated in time by the explicit Euler scheme and an explicit multistage Runge-Kutta-Chebyshev formulation of higher order, respectively.

Resolving eddy currents and the skin effect requires a suitably chosen fine spatial discretization. Since the maximum stable time step size of the explicit Euler scheme decreased quadratically for linear mesh refinements, the computation time was increased significantly. To compensate this effect of a diminished time step size, the RKC method was employed, where the maximum stable time step increase quadratically with the number of stages. The RKC method revealed a significant gain of performance over the explicit Euler scheme. The numerical tests showed that the performance of the RKC method is yet limited by the update strategy of the magnetic field dependent curl-curl matrix.

V. ACKNOWLEDGEMENT

This work was supported by the Deutsche Forschungsgemeinschaft (DFG) under grant CL143/11-2 and SCHO1562/1-2. The work of S. Schöps was supported by the Excellence Initiative of the German Federal and State Governments and the Graduate School of Computational Engineering, Technical University of Darmstadt.

REFERENCES

[1] E. Hairer, G. Wanner, "Solving Ordinary Differential Equations II", 2nd ed. Berlin, Germany, Springer, 1996.
 [2] M. Clemens, S. Schöps, H. De Gerssem, A. Bartel, "Decomposition and regularization of nonlinear anisotropic curl-curl DAEs", *COMPEL-Int. J. Comput. Math. Elect. Electron. Eng.*, vol. 30, No. 6, pp. 1701-1714, 2011.

[3] J. Dutiné, M. Clemens, S. Schöps, "Multiple Right-Hand Side Techniques in Semi-Explicit Time Integration Methods for Transient Eddy Current Problems", *IEEE Trans. Magn.*, vol. 53, No. 6, Jun. 2017.
 [4] J. Dutiné, M. Clemens, S. Schöps, "Explicit time integration of eddy current problems using a selective matrix update strategy", *COMPEL-Int. J. Comput. Math. Elect. Electron. Eng.*, vol. 36, No. 5, 2017.
 [5] B. P. Sommeijer, L. F. Shampine, J. G. Verwer, "RKC: An explicit solver for parabolic PDEs", *Elsevier Journal of Computational and Applied Mathematics*, vol. 88, pp. 315-326, 1997.
 [6] M. Clemens and T. Weiland, "Transient eddy-current calculation with the FI-method", *IEEE Trans. Magn.*, vol. 35, no. 3, pp. 1163-1166, May 1999.
 [7] T. Nakata, K. Fujiwara, "Results for benchmark problem 10 (steel plates around a coil)", *COMPEL-Int. J. Comput. Math. Elect. Electron. Eng.*, vol. 9, No. 3, pp. 181-190, Mar. 1990.
 [8] Z. Ren, "Influence of the R.H.S. on the Convergence Behaviour of the Curl-Curl Equation", *IEEE Trans. Magn.*, vol. 32, No. 3, May 1996.
 [9] Dassault Systems, CST Studio Suite 2019
 [10] T. Kolev, V. Dobrev, "Modular Finite Element Methods (MFEM)" Computer software, June 21, 2010, <https://github.com/mfem/mfem>, doi:10.11578/dc.20171025.1248.
 [11] S. Balay, S. Abhyankar et al., "Portable, Extensible Toolkit for Scientific Computation (PETSc)" Computer software, 2019, <https://www.mcs.anl.gov/petsc>